

Matrix Optimization for Poisson Compressed Sensing

Moran Mordechay and Yoav Y. Schechner

Dept. of Electrical Engineering
Technion - Israel Inst. Technology
Haifa 32000, Israel
moranmor@tx.technion.ac.il, yoav@ee.technion.ac.il

Abstract—For compressed sensing of Poissonian measurements, there is a need for nonnegative measurement matrices. We seek an optimal measurement matrix that conserves energy. Moreover, the signals pass a known but uncontrolled mixing matrix, before being multiplexed and measured. This situation is relevant to various optical applications. We optimize the measurement matrix by mutual coherence minimization, under nonnegativity and energy conservation constraints. Nonnegativity excludes the known approach of seeking an equiangular tight frame as the optimal matrix. We thus seek a quasi-equiangular frame, which is approximated by a tight frame. Simulation results demonstrate superior reconstruction using our optimized matrices, compared to random nonnegative matrices.

Index Terms—Compressed sensing, Poisson noise, Optimization, Optical imaging

I. INTRODUCTION

Analysis of compressed sensing (CS) has focused on noiseless signals or Gaussian noise [1], [2], [3], [4], [5]. For these cases, measurement matrix optimization algorithms were developed [6], [7], [8], [9], [10], [11]. Some CS works considered Poisson noise, but not matrix optimization [12], [13], [14], [15], while [16] considered impulsive noise. We consider measurement matrix optimization problem for Poisson CS. This problem is relevant to various optical applications such as hyperspectral imaging [17], [18], [19] and fluorescence microscopy [20], [21], as well as medical imaging applications such as emission tomography [12], [22], [23]. While some of these works model the noise in the measurements as Gaussian, this approximation holds only for high photon counts, otherwise the Poissonian model is more suitable [12], [19], [20].

Let $\mathbf{x} \in \mathbb{R}^m$ be an original signal, representing light intensities. We assume that \mathbf{x} is sparse, i.e., the number of its non-zero elements s' satisfies $s' \ll m$. Let there be two nonnegative matrices: $\Psi \in \mathbb{R}^{n \times m}$ and $\Phi \in \mathbb{R}^{p \times n}$, where $p \leq n \leq m$ and $p \ll m$. The acquired photon counts at the detector are $\mathbf{y} \sim \text{Poisson}(\Phi\Psi\mathbf{x}) \in \mathbb{R}^p$. Here Ψ represents uncontrolled optical mixing, such as blur, occurring before measurements are taken, while Φ is a controlled measurement matrix. A penalized maximum likelihood (ML) formulation reconstructs \mathbf{x} . We seek an optimal Φ such that the reconstruction $\hat{\mathbf{x}} \in \mathbb{R}^m$ based on \mathbf{y} estimates \mathbf{x} well. The measurement matrix Φ represents a physically feasible optical system. Hence, in addition to being nonnegative, it does not amplify energy: the total radiant energy at the output of the system Φ cannot exceed the total input energy, i.e.

$$\sum_{i=1}^p [\Phi\Psi\mathbf{x}](i) \leq \sum_{j=1}^n [\Psi\mathbf{x}](j) . \quad (1)$$

This constraint can be met by satisfying:

$$\sum_{i=1}^p \Phi(i, j) \leq 1 , \forall j . \quad (2)$$

For non-CS ($p = m$), [24], [25], [26] optimized Φ under a nonnegativity constraint. To the best of our knowledge, there has been no attempt yet to optimize Φ for CS under both nonnegativity

and energy constraints. Ref. [14] suggests using random nonnegative matrices for Poisson CS, which are not optimal. When Ψ is the identity matrix, adjacency matrices of expander graphs were also suggested as Poisson CS matrices [15]. However, expander graphs are difficult to obtain, and suitable only when Ψ is the identity matrix. Our goal is to deal with these issues.

II. MEASUREMENT MATRIX DESIGN

Considering that the measurements are noisy, it is important to avoid energy loss, since measurements with low energy have low signal-to-noise ratio (SNR). Hence, we require energy conservation, such that (2) is satisfied with equality $\forall j$. We define the set:

$$C \equiv \{ \Phi \in \mathbb{R}^{p \times n} | \Phi(i, j) \geq 0 , \forall i, j \text{ and } \sum_{i=1}^p \Phi(i, j) = 1 , \forall j \} . \quad (3)$$

Energy conservation applies to optical measurements taken by a photon sharing architecture as in [27].

The mutual coherence of $\mathbf{A} \equiv \Phi\Psi$, is [5], [28], [29]:

$$\mu(\mathbf{A}) = \max_{1 \leq i, j \leq m, i \neq j} \frac{|\mathbf{a}_i^T \mathbf{a}_j|}{\|\mathbf{a}_i\|_2 \|\mathbf{a}_j\|_2} , \quad (4)$$

where \mathbf{a}_i is column i of matrix \mathbf{A} and T denotes transposition. We aim to solve the following optimization problem:

$$\hat{\Phi} = \arg \min_{\Phi} \mu(\Phi\Psi) , \text{ s.t. } \Phi \in C . \quad (5)$$

Minimization of μ is motivated by the importance of the restricted isometry property (RIP) [4], [5], [29], [30] in Poisson CS [12], [14], and by the known relation between the RIP and μ [5], [29].

A prior attempt to minimize $\mu(\mathbf{A})$ under a nonnegativity constraint [31] solves a sequence of convex optimization problems using CVX [32]. This method is very slow, limiting its applicability to imaging and other applications which require high dimensional matrices. Our algorithm is much faster, as we detail in Sec. V.

For any $\mathbf{A} \in \mathbb{R}^{p \times m}$, the lower bound on $\mu(\mathbf{A})$ is [33], [34], [35]:

$$\mu_E = \sqrt{\frac{m-p}{p(m-1)}} . \quad (6)$$

This bound can be reached [33] if and only if \mathbf{A} is an equiangular tight frame (ETF). Frame $\mathbf{F} \in \mathbb{R}^{p \times m}$ is an equiangular frame (EF) [33], [34], if each pair of distinct columns satisfies:

$$\frac{|\langle \mathbf{f}_i, \mathbf{f}_j \rangle|}{\|\mathbf{f}_i\|_2 \|\mathbf{f}_j\|_2} = c , 1 \leq i, j \leq m , i \neq j , \quad (7)$$

where $c \in [0, 1]$ is a constant. Frame $\mathbf{F} \in \mathbb{R}^{p \times m}$ is a tight frame (TF) [33], [34], if its columns satisfy:

$$\mathbf{f} = \frac{1}{\alpha} \sum_{i=1}^m \langle \mathbf{f}, \mathbf{f}_i \rangle \mathbf{f}_i , \forall \mathbf{f} \in \mathbb{R}^p , \quad (8)$$

where α is a positive constant.

To minimize μ down to its theoretical lower bound (6), suppose we first seek an EF with $c = \mu_E$. Had it worked, then we may afterwards calculate the TF nearest to that EF, which is given [34] by a multiplication of $\mathbf{U}\mathbf{W}^T$, where $\mathbf{U}\mathbf{\Sigma}\mathbf{W}^T$ is the singular value decomposition (SVD) of that EF. This would have given us an approximated ETF.

The problem is that ETF's exist only for a few frame dimensions [33], [34]. Hence, the minimal $\mu(\mathbf{A})$ achievable is generally higher than μ_E . Furthermore, it can be shown that an EF with all nonnegative values exists only if $p = m$ or if all the columns are collinear vectors ($c = 1$). In CS, $p \ll m$. Hence, it is not possible to design Φ such that $\Phi\Psi$ is an ETF. We thus use quasi-equiangular frames (QEF). Following [36], let frame $\mathbf{F} \in \mathbb{R}^{p \times m}$ be a QEF, if each pair of distinct columns satisfies:

$$\mu_E - \varepsilon \leq \frac{|\langle \mathbf{f}_i, \mathbf{f}_j \rangle|}{\|\mathbf{f}_i\|_2 \|\mathbf{f}_j\|_2} \leq \mu_E + \varepsilon, \quad 1 \leq i, j \leq m, \quad i \neq j, \quad (9)$$

where $\varepsilon \geq 0$ is an ideally small constant. The smaller the ε parameter, the better a QEF approximates an EF with $c = \mu_E$. Therefore, instead of seeking an EF with $c = \mu_E$, which we know we cannot find, we seek a QEF with ε as small as possible, as we explain in Sec. III.

III. ALGORITHM

Inspired by [6], we use an iterative optimization algorithm. While we base our algorithm on [6], we add the constraint $\Phi \in C$, and modify the Gram matrix differently in order to achieve a QEF. We also approximate the squared root by a TF as in [11]. The following steps are executed in each iteration k of the algorithm:

- 1) Normalize the columns of the matrix $\mathbf{A}_{(k)} = \Phi_{(k)}\Psi$ to yield $\tilde{\mathbf{A}}_{(k)}$ [6], [9], [10], [11], whose i th column satisfies

$$\tilde{\mathbf{a}}_{(k),i} = \frac{\mathbf{a}_{(k),i}}{\|\mathbf{a}_{(k),i}\|_2}, \quad \forall i = 1 \dots m. \quad (10)$$

- 2) Calculate the Gram matrix of $\tilde{\mathbf{A}}_{(k)}$ [6], [9], [10], [11], defined as

$$\mathbf{G}_{(k)} = \tilde{\mathbf{A}}_{(k)}^T \tilde{\mathbf{A}}_{(k)}, \quad (11)$$

i.e., $G_{(k)}(i, j) = \langle \tilde{\mathbf{a}}_{(k),i}, \tilde{\mathbf{a}}_{(k),j} \rangle$. Note that

$$\mu(\tilde{\mathbf{A}}_{(k)}) = \max_{1 \leq i, j \leq m, i \neq j} G_{(k)}(i, j). \quad (12)$$

- 3) A parameter $\varepsilon_{(k)}$ was set in iteration $k - 1$. Define $\mu_{(k)}^t = \mu_E + \varepsilon_{(k)}$ and $\mu_{(k)}^b = \mu_E - \varepsilon_{(k)}$, where μ_E is given by (6). Then, modify $\mathbf{G}_{(k)}$ to be the Gram matrix of a QEF with parameter $\varepsilon = \varepsilon_{(k)}$, i.e.

$$\tilde{G}_{(k)}(i, j) = \begin{cases} 1 & i = j \\ \mu_{(k)}^t & i \neq j \text{ and } G_{(k)}(i, j) > \mu_{(k)}^t \\ \mu_{(k)}^b & i \neq j \text{ and } G_{(k)}(i, j) < \mu_{(k)}^b \\ G_{(k)}(i, j) & \text{otherwise} \end{cases}. \quad (13)$$

- 4) Set $\varepsilon_{(k+1)}$, such that $\varepsilon_{(k+1)} \leq \varepsilon_{(k)}$.
- 5) Find, by eigenvalue decomposition, a matrix $\mathbf{S}_{(k)} \in \mathbb{R}^{p \times m}$ such that [6], [11]

$$\tilde{\mathbf{G}}_{(k)} \approx \mathbf{S}_{(k)}^T \mathbf{S}_{(k)}. \quad (14)$$

For that, $\tilde{\mathbf{G}}_{(k)}$ should be approximated [37] by a positive semi-definite matrix with $\text{rank} \leq p$. Hence, $\mathbf{S}_{(k)}$ is an approximated QEF with parameter $\varepsilon = \varepsilon_{(k)}$.

- 6) In this step we would have calculated the TF nearest to $\mathbf{S}_{(k)}$, as explained in Sec. II and done in [11]. However, we notice that if $\mathbf{S}_{(k)}$ satisfies (14), then the matrix

$$\mathbf{S}'_{(k)} \doteq \mathbf{\Omega} \mathbf{S}_{(k)}, \quad (15)$$

also satisfies (14), where $\mathbf{\Omega}$ is any real valued $p \times p$ unitary matrix. Hence, in order to succeed better in the constrained optimization next step, we include $\mathbf{\Omega}$ in this optimization. Thus, in the current step we calculate $\mathbf{F}_{(k)}$, the TF nearest to $\mathbf{S}'_{(k)}$. We get that $\mathbf{F}_{(k)}$ is a multiplication of $\mathbf{\Omega} \tilde{\mathbf{V}}_{(k)}^T$, where $\tilde{\mathbf{V}}_{(k)}$ is a matrix whose columns are the p eigenvectors of $\tilde{\mathbf{G}}_{(k)}$, which correspond to the highest eigenvalues.

- 7) Optimize the measurement matrix $\Phi_{(k+1)}$ by solving the following optimization problem:

$$\begin{aligned} \{\Phi_{(k+1)}, \mathbf{\Omega}_{(k+1)}, w_{(k+1)}\} &= \arg \min_{\Phi, \mathbf{\Omega}, w} \|\Phi\Psi - w\mathbf{\Omega}\tilde{\mathbf{V}}_{(k)}^T\|_{\mathbb{F}}^2 \\ \text{s.t. } \Phi &\in C, \mathbf{\Omega} \in \mathcal{U}(p), w \geq \eta, \end{aligned} \quad (16)$$

where $\mathcal{U}(p)$ is the set of real $p \times p$ unitary matrices, $\eta \rightarrow 0$ is a positive constant. The variable w enables optimization which is not limited to TF of specific column norms. It is needed since for any $\mathbf{\Omega} \in \mathcal{U}(p)$, the TF $\mathbf{\Omega}\tilde{\mathbf{V}}_{(k)}^T$ has the same ℓ_2 column norms as $\tilde{\mathbf{V}}_{(k)}^T$.

Iterations yield an estimate $\hat{\Phi} \in C$, such that $\hat{\Phi}\Psi$ approximates a TF, which is also a QEF with minimal ε .

In the case where Ψ is the identity matrix, we may impose the energy conservation constraint in a simpler and more efficient way. Instead of imposing it in (16), we can multiply each column of $\hat{\Phi}$ by a different positive constant, without changing μ , and thus meet the energy conservation constraint in (3).

IV. SOLVING THE OPTIMIZATION PROBLEM (16)

The optimization problem in (16) can be approximately solved iteratively. Each iteration l solves the following subproblems:

$$\{\Phi_{(k,l+1)}, w_{(k,l+1)}\} = \arg \min_{\Phi, w} \|\Phi\Psi - w\mathbf{\Omega}_{(k,l)}\tilde{\mathbf{V}}_{(k)}^T\|_{\mathbb{F}}^2 \quad (17)$$

$$\text{s.t. } \Phi \in C, w \geq \eta.$$

$$\mathbf{\Omega}_{(k,l+1)} = \arg \min_{\mathbf{\Omega}} \|\Phi_{(k,l+1)}\Psi - w_{(k,l+1)}\mathbf{\Omega}\tilde{\mathbf{V}}_{(k)}^T\|_{\mathbb{F}}^2 \quad (18)$$

$$\text{s.t. } \mathbf{\Omega} \in \mathcal{U}(p).$$

The subproblem in (17) is convex. To solve it, we use fast iterative shrinkage-thresholding algorithm (FISTA) [38], [39]. In order to solve (17) using FISTA, the orthogonal projections of matrices, computed during iterations of FISTA, on the closed convex set C should be computed. We define the column-wise closed convex set:

$$C_{\text{col}} \equiv \{\varphi \in \mathbb{R}^p | \varphi(i) \geq 0, \forall i \text{ and } \sum_{i=1}^p \varphi(i) = 1\}. \quad (19)$$

According to (3,19), the orthogonal projection of a matrix on C can be found by projecting each column separately on C_{col} . This column-wise orthogonal projection can be calculated using the algorithm in [40].

The subproblem in (18) resembles the orthogonal Procrustes problem [41]. According to a proof in [29], as the orthogonal Procrustes problem, (18) has a closed-form solution, and this solution is as follows. Given that the SVD of the matrix $w_{(k,l+1)}\tilde{\mathbf{V}}_{(k)}^T(\Phi_{(k,l+1)}\Psi)^T$ is $\mathbf{X}_{(k,l+1)}\mathbf{Y}_{(k,l+1)}\mathbf{Z}_{(k,l+1)}^T$, we have that:

$$\mathbf{\Omega}_{(k,l+1)} = \mathbf{Z}_{(k,l+1)}\mathbf{X}_{(k,l+1)}^T. \quad (20)$$

V. SIMULATION RESULTS - NO MIXING MATRIX

In all of the tests in this section $m = 1024$, except for the comparison with [31]. Moreover, in this section we set Ψ to be the identity matrix \mathbf{I} , i.e. there is no mixing of variables. This requires $m = n$. A case where $\Psi \neq \mathbf{I}$ is treated in Sec. VI.

A. Measurement Matrix Optimization

We tested our algorithm for different values of p . As explained in Sec. III, we impose energy conservation by suitable normalization of the columns of $\hat{\Phi}$, rather than by (16). Each time, Φ was initialized by a random binary matrix [14], where 0.8 is the probability for a matrix element to be null. The algorithm ran for 300 iterations, i.e. $1 \leq k \leq 300$ (convergence was achieved much sooner). Eqs. (17,18) used 50 iterations, i.e. $1 \leq l \leq 50$. We applied FISTA with constant step size, which was chosen to be $\frac{\beta}{2\|\Psi\Psi^T\|_2}$, where $\beta \in (0, 1]$ is a constant. We let FISTA run for 6 iterations. We set $\eta = 10^{-30}$.

We initialize $\varepsilon_{(1)} = \varepsilon_{\text{init}} > 0$, and determine the value of $\varepsilon_{(k+1)}$ as follows:

$$\varepsilon_{(k+1)} = \begin{cases} \varepsilon_{\text{par}}\varepsilon_{(k)} & e_{(k)} < e_{\text{par}} \\ \varepsilon_{(k)} & \text{otherwise} \end{cases}, \quad (21)$$

where $e_{(k)}$ is the ℓ_2 norm of a vector composed of the eigenvalues of $\tilde{\mathbf{G}}_{(k)}$, which will be set to zero when finding $\mathbf{S}_{(k)}$, and $\varepsilon_{\text{par}} \in (0, 1)$ and $e_{\text{par}} > 0$ are constants. We chose $e_{\text{par}} = \tilde{e}_{\text{par}}e_{(1)}$, where $\tilde{e}_{\text{par}} \in (0, 1)$ is a constant. The rest of the parameters were chosen experimentally per p , to minimize μ . The results are shown in Table I. We also show the average mutual coherence [10], defined as:

$$\mu_{\text{avg}}(\mathbf{A}) = \frac{1}{m(m-1)} \sum_{1 \leq i, j \leq m, i \neq j} \frac{|\mathbf{a}_i^T \mathbf{a}_j|}{\|\mathbf{a}_i\|_2 \|\mathbf{a}_j\|_2}, \quad (22)$$

since the value of an average version of μ is also important for matrix reconstruction abilities [6], [7], [10]. For all our tests, also in Sec. VI, the final value of ε satisfied $\varepsilon_{(300)} > \mu_E$, meaning we would have gotten the same results without imposing $\tilde{G}_{(k)}(i, j) \geq \mu_{(k)}^b$ in step 3 of the algorithm.

TABLE I: μ_E , μ and μ_{avg} shown for different values of p , for random and optimized matrices. The parameters used are shown as well.

p/m	μ_E	μ^{rand}	μ^{opt}	$\mu_{\text{avg}}^{\text{rand}}$	$\mu_{\text{avg}}^{\text{opt}}$
0.125	0.08	0.58	0.35	0.2	0.035
0.25	0.055	0.44	0.225	0.2	0.04
0.5	0.03	0.37	0.155	0.2	0.05
p/m	β	$\varepsilon_{\text{init}}$	\tilde{e}_{par}	ε_{par}	
0.125	0.3	0.32	0.2	0.85	
0.25	0.07	0.295	0.5	0.9	
0.5	0.35	0.22	0.4	0.8	

We also compared optimization results using our algorithm, to those achieved using iterative decorrelation by convex optimization (IDCO), the algorithm of [31]. IDCO should run for a long time in order to achieve reconstruction results comparable to our algorithm. For example, when $m = 128$, $p = 64$, IDCO runs for 134 min and yields $\mu = 0.25$ and $\mu_{\text{avg}} = 0.13$, while our algorithm runs for 43 s and yields $\mu = 0.43$ and $\mu_{\text{avg}} = 0.07$. Reconstruction results are similar for both matrices. For large matrices, IDCO is impractical. For dimensions as in Table I, it would run for weeks, while our algorithm runs for less than an hour.

B. Reconstruction Results

1) Reconstruction Setting:

The reconstruction algorithm we used is the one suggested in [13], which solves a penalized ML reconstruction problem by minimizing the objective function:

$$\sum_{i=1}^p ([\mathbf{Ax}](i) - y(i) \log\{[\mathbf{Ax}](i)\}) + \tau \sum_{j=1}^m \log \left[\frac{x(j)}{\delta} + 1 \right], \quad (23)$$

subject to the nonnegativity requirement $\mathbf{x} \geq 0$, where $\tau, \delta > 0$ are constants. Ref. [13] shows that for Poissonian nonnegative signals, the penalty $\sum_{j=1}^m \log \left[\frac{x(j)}{\delta} + 1 \right]$ is more successful than the commonly used ℓ_1 norm. Eq. (23) is optimized iteratively, initialized as suggested in [14]. We set the regularization parameter to be $\tau = 0.1\|\mathbf{A}^T \mathbf{y}\|_\infty$, as suggested in [42], [43]. We initialize $\delta = 10$, and gradually increase its value during the iterations of the reconstruction algorithm. We found that this assignment of δ gives good results in a relatively short computation time.

Each matrix was normalized before the reconstruction to satisfy the energy conservation constraint in (3), as explained in Sec. III. We examined the reconstruction abilities of each matrix for three sets of random nonnegative signals \mathbf{x} . Let Λ denote such a signal set. The number of elements in the set Λ is $|\Lambda| = 100$. Each of the three signal sets has a different average sparsity percentage:

$$s = \frac{1}{|\Lambda|} \sum_{t \in \Lambda} \|\mathbf{x}_t\|_0 \cdot \frac{100}{m}. \quad (24)$$

The location of the non-zero entries in each signal is random. The value of each non-zero entry was chosen independently to be the absolute value of Gaussian random variables with zero mean and standard deviation $\sigma = 500$. Each signal was then normalized to have constant total optical energy $\|\mathbf{x}\|_1 = 0.1\sigma m$. Each test compared results based either on a random matrix or the optimized matrix.

2) The Obtained Results:

To evaluate the results, we calculate the relative error between the original and reconstructed signals by:

$$r(\mathbf{x}, \hat{\mathbf{x}}) = \|\hat{\mathbf{x}} - \mathbf{x}\|_2 / \|\mathbf{x}\|_2. \quad (25)$$

We also define the average relative reconstruction error as:

$$r_{\text{avg}}(\mathbf{x}, \hat{\mathbf{x}}) \equiv \frac{1}{|\Lambda|} \sum_{t \in \Lambda} r(\mathbf{x}_t, \hat{\mathbf{x}}_t), \quad (26)$$

and the reconstruction gain as:

$$g_{\text{rec}} \equiv r_{\text{avg}}(\mathbf{x}, \hat{\mathbf{x}}_{\text{rand}}) / r_{\text{avg}}(\mathbf{x}, \hat{\mathbf{x}}_{\text{opt}}). \quad (27)$$

Fig. 1 plots $r_{\text{avg}}(\mathbf{x}, \hat{\mathbf{x}}_{\text{rand}})$, $r_{\text{avg}}(\mathbf{x}, \hat{\mathbf{x}}_{\text{opt}})$ and g_{rec} , at different values of p and s . Increasing s reduces the reconstruction quality, since the assumption of sparse signals is less valid. When $\frac{p}{m} = 0.25, 0.5$, recovery quality considerably improves by use of optimized matrices. For less measurements, $\frac{p}{m} = 0.125$, and high s , the improvement is negligible or non-existent, and the reconstruction error is high. We conclude that even if we lower μ and μ_{avg} , there are limitations on p and s that can benefit from this optimization.

In order to assess the noise intensity in the acquired samples, we also calculate the relative measurement errors, given by $r(\mathbf{Ax}, \mathbf{y})$. For $\frac{p}{m} = 0.25$ and $\frac{p}{m} = 0.5$, $r_{\text{avg}}(\mathbf{Ax}, \mathbf{y})$ is in the range 0.03 – 0.095. In all cases, $r_{\text{avg}}(\mathbf{Ax}, \mathbf{y})$ for the optimized matrix is smaller than $r_{\text{avg}}(\mathbf{Ax}, \mathbf{y})$ for the random matrix, even though the optimized matrices were not directly designed to fulfill such a requirement. This is an indicator that an optimized matrix reduces $r_{\text{avg}}(\mathbf{Ax}, \mathbf{y})$, probably because of two reasons. First, the optimized matrix is sparser than the random one. Second, the position of non-zero elements in an optimized matrix is not random. Both reasons appear to concentrate the signal energy in fewer elements of \mathbf{Ax} for the optimized matrix, with higher values.

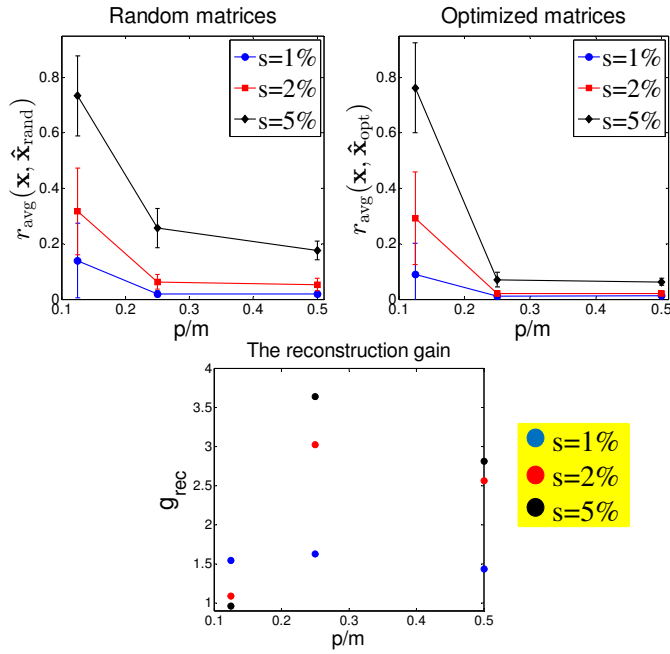


Fig. 1: The average relative reconstruction errors and the reconstruction gain. For low p , $p = 128$ ($\frac{p}{m} = 0.125$), $r_{\text{avg}}(\mathbf{x}, \hat{\mathbf{x}})$ is very high, for both the random and optimized matrices. However, when there are enough measurements, optimized measurement matrices considerably improve recovery quality.

VI. SIMULATION RESULTS - AVERAGING BLUR MIXING

We tested our algorithm when Ψ is a square matrix whose operation on \mathbf{x} is¹

$$[\Psi\mathbf{x}](i) = [x(i-1) + x(i) + x(i+1)]/3, \forall i, \quad (28)$$

i.e. Ψ is an averaging blur. We keep the number of measurements constant $p = 256$, and test our algorithm for different $m = n$ values. We use the same simulation setting as in Sec. V, except that energy conservation is imposed in (16), and Φ is initialized by a random normalized matrix. The measurement matrix optimization results are shown in Table II. The values of g_{rec} are shown in Table III. In all cases shown in Table III, the use of optimized matrices improves the reconstruction quality. Also here $r_{\text{avg}}(\mathbf{A}\mathbf{x}, \mathbf{y})$ is lower for the optimized matrices, since an optimized Φ yields a sparser \mathbf{A} with less random arrangement of non-zero elements. Fig. 2 shows an example of the reconstruction results for $m = 1024$ ($\frac{p}{m} = 0.25$) and $s' = 22$, when using random and optimized matrices.

TABLE II: μ_E , μ and μ_{avg} shown for different values of m , for random and optimized matrices, and refer to $\mathbf{A} = \Phi\Psi$. Here Ψ represents averaging blur. The parameters used are shown as well, in all the tests $\tilde{\epsilon}_{\text{par}} = 0.7$ and $\epsilon_{\text{par}} = 0.9$.

p/m	μ_E	μ^{rand}	μ^{opt}	$\mu_{\text{avg}}^{\text{rand}}$	$\mu_{\text{avg}}^{\text{opt}}$	β	ϵ_{init}
0.2	0.056	0.90	0.78	0.425	0.06	0.27	0.44
0.25	0.055	0.88	0.82	0.425	0.07	0.78	0.445
1/3	0.05	0.885	0.79	0.42	0.09	0.31	0.55
0.5	0.045	0.92	0.85	0.43	0.1	0.23	0.555

¹For $i = 1$ we used $x(i-1) = 0$, and for $i = m$ we used $x(i+1) = 0$.

TABLE III: The reconstruction gain when there is averaging blur before the measurements are taken.

p/m	$s = 1\%$	$s = 2\%$	$s = 5\%$
0.2	4.3	3.7	2.5
0.25	4.3	3.9	3.1
1/3	3.65	4.2	3.3
0.5	2	2.3	2.7

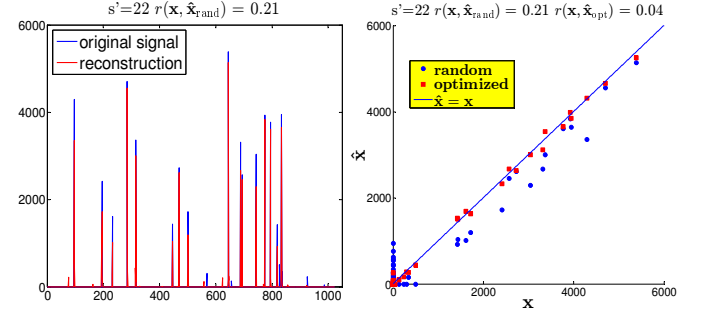


Fig. 2: Example of original and reconstructed signals for $m = 1024$ using the random matrix, and the scatter plots for both the random and optimized matrices. There are 22 non-zeros in \mathbf{x} . The optimized matrix considerably improves reconstruction accuracy, as evident from the scatter plots.

VII. CONCLUSIONS

We presented a measurement matrix optimization algorithm for Poisson compressed sensing. The optimization is done by mutual coherence minimization, under the constraint of nonnegativity and energy conservation. Simulation results demonstrate superior reconstruction using our optimized matrices, compared to random nonnegative matrices. This work is relevant to various optical applications. Since our algorithm is not guaranteed to converge to a global optimum, matrix optimization results depend on the initial random matrix chosen. It would be interesting to explore stochastic global optimization methods to escape local minima. We assume that the signals are sparse in the canonical basis. However, our algorithm can be generalized to sparsity in some noncanonical basis or dictionary \mathbf{D} [6], [7], [8], [9], [10], [11], by compounding \mathbf{D} with the mixing matrix Ψ , resulting in $\tilde{\Psi} = \Psi\mathbf{D}$. Additional modifications might be needed, since $\tilde{\Psi}$ is not necessarily nonnegative. Energy conservation makes our matrices suitable for photon sharing architectures. In serial sensing as [44], energy is not conserved, as signal modulation decreases the energy of each signal element. Then, energy conservation must not be imposed on the optimization. Instead, it is advisable to include the Poisson noise model directly in the matrix optimization.

ACKNOWLEDGEMENT

We thank Michael Elad, Yonina Eldar and the anonymous reviewers for their useful comments and Amir Beck for his suggestions regarding optimization methods. Yoav Schechner is a Landau Fellow - supported by the Taub Foundation. The work was supported by the E. and J. Bishop Research Fund and Israel Science Foundation (ISF Grant 1467/12). This work was conducted in the Ollendorff Minerva Center. Minerva is funded through the BMBF.

REFERENCES

- [1] E. J. Candès, J. Romberg, and T. Tao, "Robust uncertainty principles: Exact signal reconstruction from highly incomplete frequency informa-

- tion," *IEEE Transactions on Information Theory*, vol. 52, no. 2, pp. 489 – 509, February 2006.
- [2] E. J. Candès and T. Tao, "Near optimal signal recovery from random projections: Universal encoding strategies?" *IEEE Transactions on Information Theory*, vol. 52, no. 12, pp. 5406 – 5425, December 2006.
 - [3] D. Donoho, "Compressed sensing," *IEEE Transactions on Information Theory*, vol. 52, no. 4, pp. 1289 – 1306, April 2006.
 - [4] E. J. Candès and M. B. Wakin, "An introduction to compressive sampling," *IEEE Signal Processing Magazine*, vol. 25, no. 2, pp. 21 – 30, March 2008.
 - [5] M. Duarte and Y. C. Eldar, "Structured compressed sensing: From theory to applications," *IEEE Transactions on Signal Processing*, vol. 59, no. 9, pp. 4053 – 4085, September 2011.
 - [6] M. Elad, "Optimized projections for compressed sensing," *IEEE Transactions on Signal Processing*, vol. 55, no. 12, pp. 5695 – 5702, December 2007.
 - [7] J. M. Duarte-Carvajalino and G. Sapiro, "Learning to sense sparse signals: Simultaneous sensing matrix and sparsifying dictionary optimization," *IEEE Transactions on Image Processing*, vol. 18, no. 7, pp. 1395 – 1408, July 2009.
 - [8] W. Chen, M. R. D. Rodrigues, and I. J. Wassell, "Projection design for statistical compressive sensing: A tight frame based approach," *IEEE Transactions on Signal Processing*, vol. 61, no. 8, pp. 2016 – 2029, April 2013.
 - [9] J. Xu, Y. Pi, and Z. Cao, "Optimized projection matrix for compressive sensing," *EURASIP Journal on Advances in Signal Processing*, vol. 2010, p. 43, 2010.
 - [10] V. Abolghasemi, S. Ferdowsi, and S. Sanei, "A gradient-based alternating minimization approach for optimization of the measurement matrix in compressive sensing," *Signal Processing*, vol. 92, no. 4, pp. 999 – 1009, 2012.
 - [11] E. Tsiligiani, L. P. Kondi, and A. K. Katsaggelos, "Use of tight frames for optimized compressed sensing," in *Proceedings of the 20th European Signal Processing Conference (EUSIPCO)*, August 2012, pp. 1439–1443.
 - [12] Z. T. Harmany, R. F. Marcia, and R. M. Willett, "This is spiral-tap: Sparse poisson intensity reconstruction algorithms: Theory and practice," *IEEE Transactions on Image Processing*, vol. 21, no. 3, pp. 1084 – 1096, March 2012.
 - [13] D. J. Lingenfelter, J. A. Fessler, and Z. He, "Sparsity regularization for image reconstruction with poisson data," in *IS&T/SPIE Electronic Imaging*, vol. 7246, 2009, pp. 72460F–1–72460F–10.
 - [14] M. Raginsky, Z. T. Harmany, R. F. Marcia, and R. M. Willett, "Compressed sensing performance bounds under poisson noise," *IEEE Transactions on Signal Processing*, vol. 58, no. 8, pp. 3990 – 4002, 2010.
 - [15] M. Raginsky, S. Jafarpour, Z. T. Harmany, R. F. Marcia, R. M. Willett, and R. Calderbank, "Performance bounds for expander-based compressed sensing in poisson noise," *IEEE Transactions on Signal Processing*, vol. 59, no. 9, pp. 4139 – 4153, September 2011.
 - [16] A. B. Ramirez, G. R. Arce, D. Otero, J. L. Paredes, and B. M. Sadler, "Reconstruction of sparse signals from ℓ_1 dimensionality-reduced cauchy random projections," *IEEE Transactions on Signal Processing*, vol. 60, no. 11, pp. 5725 – 5737, November 2012.
 - [17] G. R. Arce, D. J. Brady, L. Carin, H. Arguello, and D. S. Kittle, "Compressive coded aperture spectral imaging: An introduction," *IEEE Signal Processing Magazine*, vol. 31, no. 1, pp. 105–115, January 2014.
 - [18] Y. August, C. Vachman, Y. Rivenson, and A. Stern, "Compressive hyperspectral imaging by random separable projections in both the spatial and the spectral domains," *Applied optics*, vol. 52, no. 10, pp. D46–D54, April 2013.
 - [19] R. Willett, M. Duarte, M. Davenport, and R. Baraniuk, "Sparsity and structure in hyperspectral imaging: Sensing, reconstruction, and target detection," *IEEE Signal Processing Magazine*, vol. 31, no. 1, pp. 116–126, January 2014.
 - [20] V. Studer, J. Bobin, M. Chahid, H. S. Mousavi, E. Candès, and M. Dahan, "Compressive fluorescence microscopy for biological and hyperspectral imaging," *Proceedings of the National Academy of Sciences*, vol. 109, no. 26, pp. E1679–E1687, 2012.
 - [21] S. Schwartz, A. Wong, and D. A. Clausi, "Compressive fluorescence microscopy using saliency-guided sparse reconstruction ensemble fusion," *Optics Express*, vol. 20, no. 16, pp. 17281–17296, July 2012.
 - [22] S. Valiollahzadeh, T. Chang, J. W. Clark, and O. R. Mawlawi, "Image recovery in pet scanners with partial detector rings using compressive sensing," in *2012 IEEE Nuclear Science Symposium and Medical Imaging Conference (NSS/MIC)*, 2012, pp. 3036 – 3039.
 - [23] G. Chinn, P. D. Olcott, and C. S. Levin, "Improved compressed sensing multiplexing for pet detector readout," in *2012 IEEE Nuclear Science Symposium and Medical Imaging Conference (NSS/MIC)*, 2012, pp. 2472–2474.
 - [24] N. Ratner and Y. Y. Schechner, "Illumination multiplexing within fundamental limits," in *IEEE Conference on Computer Vision and Pattern Recognition, 2007. CVPR'07*, 2007, pp. 1–8.
 - [25] N. Ratner, Y. Y. Schechner, and F. Goldberg, "Optimal multiplexed sensing: bounds, conditions and a graph theory link," *Optics express*, vol. 15, no. 25, pp. 17072–17092, December 2007.
 - [26] M. Alterman, Y. Y. Schechner, and A. Weiss, "Multiplexed fluorescence unmixing," in *2010 IEEE International Conference on Computational Photography (ICCP)*, 2010, pp. 1–8.
 - [27] M. A. Neifeld and J. Ke, "Optical architectures for compressive imaging," *Applied optics*, vol. 46, no. 22, pp. 5293–5303, August 2007.
 - [28] D. Donoho and M. Elad, "Optimally sparse representation in general (nonorthogonal) dictionaries via ℓ_1 minimization," *Proceedings of the National Academy of Sciences*, vol. 100, no. 5, pp. 2197–2202, March 2003.
 - [29] M. Elad, *Sparse and redundant representations: from theory to applications in signal and image processing*. Springer, 2010.
 - [30] E. J. Candès, J. Romberg, and T. Tao, "Stable signal recovery from incomplete and inaccurate measurements," *Communications on Pure and Applied Mathematics*, vol. 59, no. 8, pp. 1207 – 1223, August 2006.
 - [31] C. Rusu, "Design of incoherent frames via convex optimization," *IEEE Signal Processing Letters*, vol. 20, no. 7, pp. 673 – 676, July 2013.
 - [32] M. Grant and S. Boyd, "CVX: Matlab software for disciplined convex programming, version 2.0 beta," <http://cvxr.com/cvx>, 2013.
 - [33] T. Strohmer and R. W. Heath, "Grassmannian frames with applications to coding and communication," *Applied and Computational Harmonic Analysis*, vol. 14, no. 3, pp. 257 – 275, 2003.
 - [34] J. A. Tropp, I. S. Dhillon, R. W. Heath, and T. Strohmer, "Designing structured tight frames via an alternating projection method," *IEEE Transactions on Information Theory*, vol. 51, no. 1, pp. 188–209, January 2005.
 - [35] L. R. Welch, "Lower bounds on the maximum cross correlation of signals," *IEEE Transactions on Information Theory*, vol. 20, no. 3, pp. 397 – 399, May 1974.
 - [36] H. Shi, H. Zhang, and X. Wang, "Quasi-equiangular frames (QEFs): A new flexible configuration of frames," *arXiv preprint arXiv:1301.6318*, 2013.
 - [37] R. Horn and C. Johnson, *Matrix Analysis*. Cambridge University Press, 1985.
 - [38] A. Beck and M. Teboulle, "A fast iterative shrinkage-thresholding algorithm for linear inverse problems," *SIAM Journal on Imaging Sciences*, vol. 2, no. 1, pp. 183 – 202, March 2009.
 - [39] A. Beck and M. Teboulle, "Fast gradient-based algorithms for constrained total variation image denoising and deblurring problems," *IEEE Transactions on Image Processing*, vol. 18, no. 11, pp. 2419–2434, November 2009.
 - [40] R. Helgason, J. Kennington, and H. Lall, "A polynomially bounded algorithm for a singly constrained quadratic program," *Mathematical Programming*, vol. 18, no. 1, pp. 338–343, 1980.
 - [41] P. H. Schönemann, "A generalized solution of the orthogonal procrustes problem," *Psychometrika*, vol. 31, no. 1, pp. 1 – 10, March 1966.
 - [42] M. A. T. Figueiredo, R. D. Nowak, and S. J. Wright, "Gradient projection for sparse reconstruction: Application to compressed sensing and other inverse problems," *IEEE Journal of Selected Topics in Signal Processing*, vol. 1, no. 4, pp. 586 – 597, December 2007.
 - [43] S. Kim, K. Koh, M. Lustig, S. Boyd, and D. Gorinevsky, "An interior-point method for large-scale ℓ_1 -regularized least squares," *IEEE Journal of Selected Topics in Signal Processing*, vol. 1, no. 4, pp. 606–617, December 2007.
 - [44] M. F. Duarte, M. A. Davenport, D. Takhar, J. N. Laska, T. Sun, K. F. Kelly, and R. G. Baraniuk, "Single-pixel imaging via compressive sampling," *IEEE Signal Processing Magazine*, vol. 25, no. 2, pp. 83–91, March 2008.